**THE EUROPEAN
PHYSICAL JOURNAL D**

Regular Article

Measurement of the force exerted on the surface of an object immersed in a plasma

Thomas Trottenberg[a], Thomas Richter, and Holger Kersten

Institut für Experimentelle und Angewandte Physik, Christian-Albrechts-Universität zu Kiel, 24098 Kiel, Germany

Abstract. An experiment is described in which the force exerted by a low-pressure rf plasma on one side of a test surface is measured. The test surface is part of a cubic object immersed in the plasma and is mounted on a pendulum whose small deviations are recorded by a digital camera. The force balance is calibrated by means of an electrostatic method. The measured forces on the surface ($4.8\,\mathrm{cm}^2$) are in the micronewton range and increase with the plasma density, while an increased collisionality reduces the force. The measured forces are discussed on the basis of a simple model taking into account the momentum fluxes across the sheath edge. It is concluded that ion-neutral collisions in the presheath enhance the force caused by electron pressure and ion flux.

1 Introduction

Plasma-wall interactions in low-temperature plasmas are usually considered with respect to electric currents and heat flux to the wall, sputtering, ion implantation, deposition, secondary electron emission and surface reactions, to mention the most important aspects. In contrast, the forces that plasmas exert on walls have never been a major topic. This contribution aims at a demonstration, that the forces related to plasma-wall interactions are experimentally accessible with some effort.

Force measurements could provide valuable information about the composition of the impinging particles and their velocity distributions. This becomes clear when one contemplates the measured quantities in case of electrostatic and force probe measurements. In case of electrostatic methods, e.g. Langmuir probes, Faraday cups, and retarding field probes, a current is measured that results from collected charged particles. The current can be written based on the velocity distribution function $f(v_x)$ in front of the probe, which for the sake of convenience is here simplified to one dimension with the velocity coordinate v_x perpendicular to the small surface A. The current is:

$$I = A \sum_{j=\mathrm{i,e}} q_j \int\limits_{-\infty}^{+\infty} v_x f_j(v_x) dv_x, \qquad (1)$$

where q_j are the particles' charges of, for simplicity, singly charged ions, $j = \mathrm{i}$, and electrons, $j = \mathrm{e}$. Note that these velocity distribution functions $f_j(v_x)$ are not the ones in the plasma, but the disturbed functions directly in front of the collecting surface. In particular, the distributions

are non-Maxwellian and asymmetric, e.g. because of losses and inelastic collisions at the wall, electric fields and production of secondary electrons. On the other hand, a force probe measures

$$F = A \sum_{j=\mathrm{i,e,n}} m_j \int\limits_{-\infty}^{+\infty} v_x^2 f_j(v_x) dv_x + F_E, \qquad (2)$$

where this time neutral atoms, $j = \mathrm{n}$, come into play: the force probe is not sensitive only to charged particles, but also to neutral atoms. Additionally, an electrostatic force F_E (electrostatic stress) is pulling the surface toward the plasma. However, this is not the only difference. The integral in equation (2) is now the *second moment* of the distribution function f_j, while in equation (1) it was the *first moment*, i.e. the weighting by the velocities is different.

From the viewpoint of momenta of velocity distribution functions, a third kind of probes should be mentioned: Recently, calorimetric probes have increasingly been applied for plasma diagnostics [1–5]. Here, the corresponding integral is *a third moment* of the (three-dimensional) velocity distribution function; however, additional contributions, for example from chemical reactions, condensation and film deposition, evaporation and sputtering, heat conduction, and radiation, may play an important role.

In our laboratory at the University of Kiel, we are currently working on experiments for the study of plasma sheaths by means of a combination of electrostatic, calorimetric and force measuring techniques. Those investigations aim at a better understanding of gas heating by a plasma [6–10], the momentum transfer from ions to the neutral gas in the presence of electric fields [11,12],

ᵃ e-mail: `trottenberg@physik.uni-kiel.de`
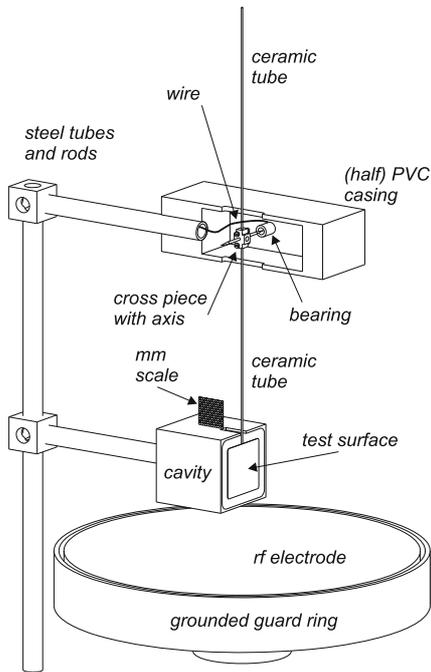
Fig. 1. Experimental setup. The cubic cavity excludes the plasma from behind the test surface. The front part of the PVC casing is not drawn in favor of its inside.

and of plasma sheaths in case of single and multiple ion species plasmas [13–17].

In this article, we describe our first experiment that demonstrates the feasibility of a force probe for plasma diagnostics. The paper is organized as follows. A description of the experimental setup is given in Section 2, while the following Section 3 is dedicated to the calibration of the force probe. Measurement results and their discussion follow in Section 4, before the Conclusions summarize the open questions and propose further experiments.

2 Experimental setup

The experimental setup is a typical capacitively coupled asymmetric rf discharge configuration with a powered horizontal electrode and the vacuum chamber as grounded counter electrode. The rf electrode is a stainless steel disk of 14 cm diameter surrounded by a grounded guard ring (see Fig. 1). The cylindrical vacuum vessel has a diameter of 30 cm and a height of 26 cm. The discharge is operated with argon at three different pressures $p = (5, 10, 20)$ Pa and rf powers in the range of $P = (20-300)$ W at a frequency of 13.56 MHz.

Figure 1 shows the rf electrode with the pendulum force probe and an aluminum cavity behind the probe surface. The cavity has the purpose to exclude the plasma from the volume behind the probe surface. Both the cavity and the polyvinyl chloride (PVC) casing for the pendulum axis are supported by an arrangement of steel tubes and rods from the bottom of the vacuum chamber. The rods and the cavity can be grounded, otherwise they

are floating. The position of the center of the test surface was about 40 mm above the center of the electrode. Between the edges of the 4.8 cm^2 surface and the inner edges of the cavity is a gap of approximately 4 mm.

The pendulum consists of two approximately 100 mm long ceramic tubes, where the test surface is attached to the end of the lower lever arm; the upper arm serves as a counter weight. The two lever arms are joined at the rotational axis in a small cross piece. The rotational axis is realized by a steel rod tapered at both ends and led through the cross piece perpendicularly to the ceramic tubes. The axis is pivot-mounted in two conical metal bearings.

The test surface is made of 0.02 mm thick steel sheet and has a square shape (edge length 22 mm) with rounded vertices. A thin wire is soldered to the rear side of the surface. The wire is led through the ceramic tube and from there to the axis which is in electric contact with the bearings. The bearings for their part are connected by means of an isolated wire in the inner of the supporting steel tubes to a vacuum feedthrough which allows biasing of the test surface. The dielectric casing shields the cross piece, the axis and the bearings from the plasma.

A slit in the upper side of the cavity cube allows the pendulum to move inward. The measurement of the pendulum deflection is done with the help of a CMOS camera that looks through a window in the vacuum chamber in a direction parallel to the pendulum's rotational axis. The field of view includes the ceramic lever arm where it passes through the cavity's slit and a millimeter scale mounted on top of the cavity. From the 2816×2112 pixel images, the deflection of the observed point on the lever arm is determined (the deflection of the test surface is greater by a factor of 1.22 due to its longer distance from the axis).

The plasma was characterized by rf-compensated Langmuir probe measurements 1 cm in front of the test surface [18–20]. The cylindrical probe, with a 100 μm tungsten wire of (3.0 ± 0.2) mm length as active probe tip at the end of a thin ceramic tube, is passively filtered at the rf frequency and its first harmonic, and is biased via a capacitor by a reference electrode that picks up the rf plasma potential variations. In our design, the reference electrode is a 10 mm long copper tube mounted at the end of another thin ceramic tube parallel to the first one, at a distance of about 5 mm from the probe tip.
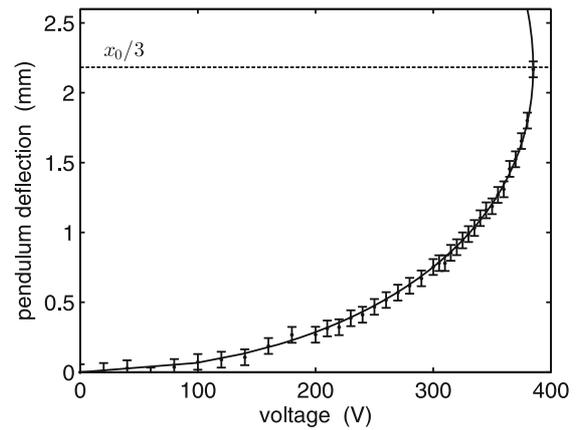
3 Calibration

The calibration of the force probe is done by means of an electrostatic method. The main idea is to complement the test surface by a second surface of the same size to obtain a parallel plate capacitor, as shown in Figure 2. Application of a voltage between the test surface and the counter electrode generates an attractive force that will deflect the pendulum until an equilibrium, if it exists, is reached.

The attractive force between the plates is approximately $F_{\mathrm{attr}} = \frac{1}{2} A \epsilon_0 E^2$ for distances that are small in comparison to the plate size. This can be written with
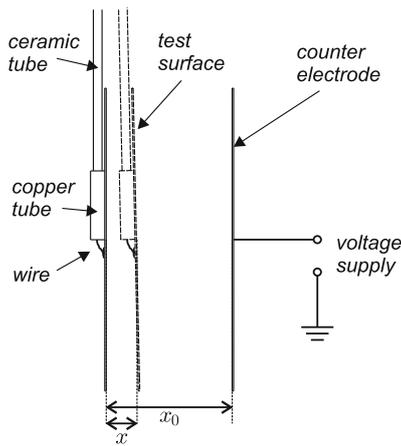
Fig. 2. Setup for the calibration. A counter electrode complements the test surface to a capacitor. The displacement of the test surface due to the electrostatic attraction between both plates is recorded by a camera (not shown).

Fig. 3. Example of a calibration measurement. The deflections of the pendulum are recorded for different voltages (see Fig. 2). For deflections higher than $1/3$ of the initial plate distance, the pendulum becomes unstable.

the help of the applied voltage U and the initial plate distance x_0 as a function of the deflection $x = (0 \ldots x_0)$ from the initial position:

$$F_{\mathrm{attr}}(x) = \frac{1}{2} A \epsilon_0 \frac{U^2}{(x_0 - x)^2}. \tag{3}$$

The plates touch each other at $x = x_0$.

The restoring force of the pendulum is in the small-angle approximation $F_{\mathrm{rest}}(x) = -D\,x$, with the "spring constant" D as the deflection-to-force conversion factor that has to be determined by the calibration. The equilibrium requires

$$\frac{1}{2} A \epsilon_0 \frac{U^2}{(x_0 - x)^2} + D\,x = 0. \tag{4}$$

For the calibration, the equlibrium deflections x for several voltages U are measured. Figure 3 shows such a calibration together with the best fit using D and x_0 as free parameters.

At $x/x_0 = 1/3$ the pendulum becomes unstable, i.e. a small (positive) deflection brings it into a position from where on the attractive force is higher than the restoring force, and the plates snap together. This is the reason, why only measurements for $x < x_0/3$ are shown in Figure 3. In order to avoid a short-circuit, the current was limited by a 100 kΩ resistor.

A series of measurements begins with small voltages and proceeds in decreasing steps until the critical voltage is reached. Four of such calibration series have been recorded for two different initial distances x_0 for positive and negative voltages, respectively. The resulting calibration constant is $D = (7.8 \pm 1.5)\ \mu\mathrm{N/mm}$. (The respective fit parameters x_0 have been checked for plausibility with a caliper).

We compared the experimentally determined value for D with the expected value from a simple model of the pendulum taking into account the calculated masses

of the test surface, the copper tube and the wire. The estimated value is about 20 percent higher than the one obtained from the calibration and has itself an error of at least 15 percent due to the material tolerances. Therefore, the estimation is in good agreement with the calibration.

The force F can now be calculated from the observed deflections x by means of the equation

$$F(x) = D\,x. \tag{5}$$

4 Measurements and discussion

Three series of force measurements have been performed, each one at one of the argon gas pressures $p = (5, 10, 20)$ Pa. For each series, the rf powers have been increased from $P = 20$ W to $P = 300$ W by steps of 20 W. For each pressure-power parameter pair, two positions have been measured from which the deflection was determined: the position with the discharge switched off and the position with the discharge switched on.

Figure 4 shows the deflections for a grounded and a floating test surface (the cavity is also grounded or floating, respectively). The deflections of the test surface are always directed into the cavity, i.e. the measured forces have the direction from the plasma to the surface. The forces calculated from the deflections with the help of equation (5) are displayed in Figure 5. Error bars result mainly from the error in D, but also from the repeatability of the deflection measurements (error bars in Fig. 4).

Two trends can be identified: firstly, the force increases when the discharge power is increased, and, secondly, the force decreases when the gas pressure is increased. Moreover, no significant difference is found between the grounded and the floating surface.

In order to gain an understanding of the mechanism that causes the forces, we performed Langmuir probe measurements at a distance of 1 cm in front of the test surface. The main plasma parameters can be summarized as follows: There are no significant differences between
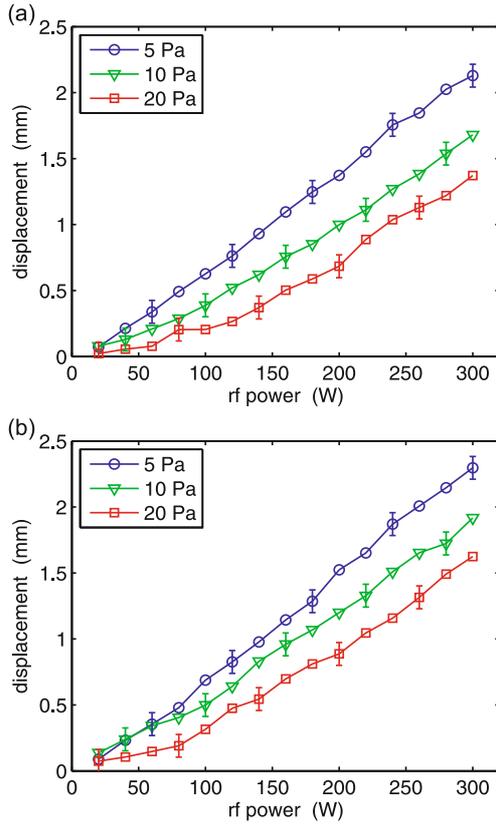
Fig. 4. Measured displacements of the grounded (a) and the floating (b) test surfaces.
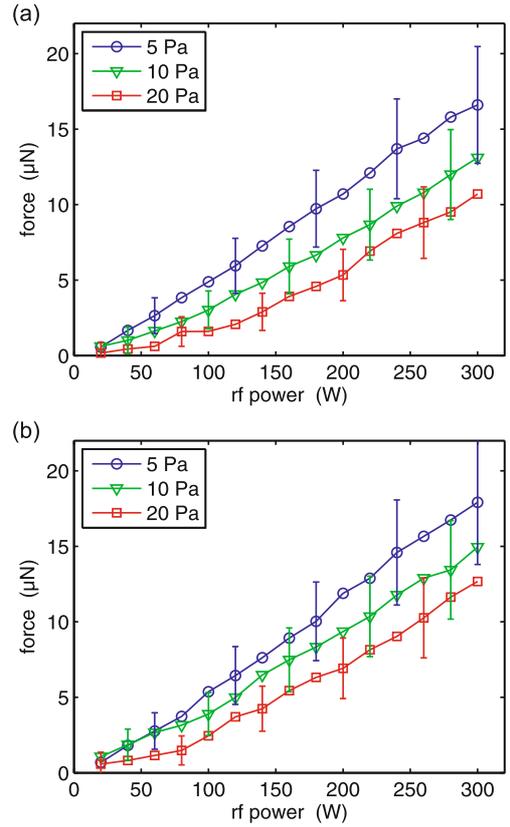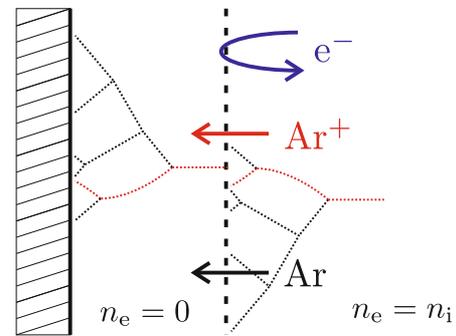

Fig. 5. Measured forces on the grounded (a) and the floating (b) test surfaces. The cavity is grounded or floating, too.

Fig. 6. Sketch of the momentum fluxes across the sheath edge. The dashed line separates the quasi-neutral plasma, including presheath, from the virtually electron-free sheath. The dotted lines represent collision cascades in the sheath and the presheath.

the cases where the cavity and test surface are grounded or floating. The densities increase continuously when the rf power is increased and reach $(9.6, 13, 20) \times 10^{15}$ m^{-3} ($\pm 30\%$) at 300 W for the three pressures $p = (5, 10, 20)$ Pa. The electron temperatures increase for the corresponding powers from 2.0 to 4.0 eV (± 0.5 eV) with no difference between the three pressures. The plasma potential U_{pl} develops smoothly between 20 and 22 V (± 0.5 V) for $p = 5$ Pa, between 21 and 23 V for $p = 10$ Pa, and between 23 and 26 V for $p = 20$ Pa.

The similarity of the plasma parameters for the grounded and the floating setup is in agreement with only little changes in the visible plasma glow. We conclude from these facts that even in the grounded case the effective counter electrode is still the vacuum chamber and not, as one could expect, predominantly the cavity, test surface and rods, which are relatively close to the rf electrode. In a big chamber with the walls well-separated from the plasma, the discharge would be asymmetric with a strong rf sheath at the grounded parts. In our case, the chamber walls are in good contact with the plasma which visibly fills the entire chamber, so that similar sheaths develop in front of all the walls, and strong potential differences between the walls and the introduced floating parts cannot build up.

The understanding of the measured forces in the order of magnitude of several micronewtons is by no means trivial, as the following discussion will show. For this

purpose, we roughly divide the space in front of the surface in the electron-free sheath and the quasi-neutral plasma, including the presheath (see Fig. 6).

First, the electron pressure. Only a negligible fraction of the electrons reaches the test surface which is in the time average at a potential a several times $k_{\mathrm{B}}T_{\mathrm{e}}/e$ below the plasma potential, where k_{B} is the Boltzmann constant and e is the elementary charge. In case of a floating test surface, the potential is $\Phi_{\mathrm{float}} \approx -4.7 k_{\mathrm{B}}T_{\mathrm{e}}/e$ relative to the plasma, assuming a Maxwellian energy distribution

for the electrons and ions entering the sheath at the Bohm speed $v_B = (k_B T_e / m_i)^{1/2}$, where m_i is the mass of an argon ion. The grounded surface is at the potential $\Phi_{\text{float}} = -U_{\text{pl}}$, which obviously does not deviate much from the floating potential.

In this situation, nearly all the electrons are reflected in the sheath, so that the electron pressure at the sheath edge acts on the charges which generate the electric field in the sheath. The sheath is electrostatically made up of ions, and therefore, the electron pressure transfers momentum to the ions in the sheath and the surface charges on the test surface. This means, that the momentum will directly or indirectly reach the test surface. We conclude therefore, that the electron pressure is one of the components of the measured force. The electron pressure is:

$$p_e = k_B T_e n_s, \qquad (6)$$

where $n_s = \exp(-1/2) n_e$ is the electron density at the sheath edge, which is in case of a collisionless sheath by the factor of $\exp(-1/2) \approx 0.6$ lower than the density n_e measured in the plasma. Figure 7 shows the resulting forces $F_e = p_e A$ for the two pressures $p = 5$ and 20 Pa as dotted lines. The electron pressure can explain almost half of the force in the 20 Pa case, but significantly less in the 5 Pa case.

Second, the momentum that the ions bring into the sheath. Assuming a collisionless presheath, the momentum of an ion entering the sheath is $v_B m_i$ and the flux density is $v_B n_s$. However, in case of a collisional presheath, the ion speed will be smaller than the Bohm speed [21]. Therefore, the momentum flux density, with the unit of a pressure, yields an upper limit for the "ion pressure" in our collisional plasma:

$$p_i \le k_B T_e n_s. \qquad (7)$$

In the following, we discuss the momentum that the ions additionally gain in the electric field of the sheath and the electrostatic force that pulls the surface.

Under the assumption that the electric field in the sheath vanishes at the sheath edge and that the sheath is free of electrons, which is only a simplified picture, there is no further momentum transfer via electric fields or charged particles across the sheath edge. Therefore, according to Newton's third law, the force that accelerates the ions toward the surface equals the force pulling the surface toward the plasma, since all the field lines emerge from the ions and end at the surface. Hence, the momentum gained by the ions in the sheath, which will be transferred to the surface when the ions impinge there, was previously taken from the surface, so that both forces cancel each other out and can be omitted in the force balance if the entire momentum of the ions finally reaches the surface. This balance of forces in the sheath has another important implication for the force exerted on the surface. In simple theories, e.g. electron-free collisionless Child-Langmuir sheath and collisional sheath, the wall potential determines the sheath width, but the presheath, expecially the ion flux and the sheath entry velocity of the ions remain unaffected. Therefore, moderate biasing
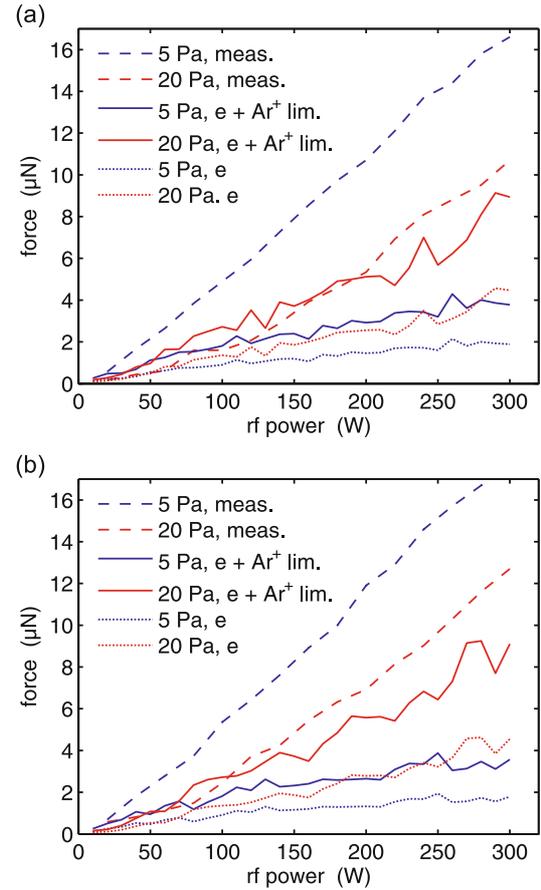
Fig. 7. Comparison of the measured forces on the grounded (a) and floating (b) surfaces with the corresponding calculated forces due to electron pressure and ions streaming into the sheath. For the ions, Bohm velocity was assumed, so that the continuous lines indicate upper limits for the collisional cases.

the surface should not have much influence on the measured force, and that is what the measurements with the grounded and the floating surface show. The applicability of our simplified picture certainly ends, when the wall potential approaches $\Phi_w \approx -kT_e/e$. Then, a strong electron current across the sheath will not only be absorbed at the surface and reduce the electron pressure, it will also change the plasma in front of the surface.

However, two effects make the situation more complicated. The first effect arises from ion-neutral collisions. Such collisions (unless they involve excitation and emission of a photon) conserve the momentum, especially the momentum normal to the surface is conserved which contributes to the measured force. In such a binary collision, the normal momentum is split into two smaller parts for each of the two collision partners. The first collision of the ion initiates a collision cascade as indicated in Figure 6. If not so many collisions occur that the energy of the knocked-on gas atoms drops below the thermal energy, the momentum gained by the ions in the field finally reaches the surface. Otherwise the momentum could, due to diffusion, be transported away from the surface.

In the $p = 5$ Pa case, the momentum exchange mean free path for ions at Bohm speed, which is the characteristic speed for the sheath, is $\lambda_{\mathrm{mfp}} \approx 0.8$ mm [22] which is approximately the sheath width $d \approx 0.7$ mm for the Child-Langmuir sheath and $d \approx 0.8$ mm for the collisional sheath, calculated with the respective measured plasma parameters at $P_{\mathrm{rf}} = 300$ W. This means, that an average ion in the sheath transfers once its momentum to a gas atom ($d/\lambda_{\mathrm{mfp}} \approx 1$). Since the ion gained energy in the order of magnitude of electronvolts, all the collision partners in the cascade are superthermal. In case of $p = 20$ Pa, the momentum exchange mean free paths are $\lambda_{\mathrm{mfp}} \approx 0.2$ mm and the sheath lengths are $d \approx 0.5$ mm for both models. This time, $d/\lambda_{\mathrm{mfp}} \approx 2.5$, so that the collision cascade will have two or three generations with four to eight particles. Even in this case, the energy per particle is much higher than the mean thermal energy of the gas atoms, and the cascade ends at the surface.

The other complicating effect arises from reflections at the surface. If the impinging ions and knocked-on atoms do not accommodate at the surface, i.e. the released particles carry away a significant amount of momentum, there would be additional repulsion. Experimental data show typical normal momentum accommodation coefficients above 0.8 for perpendicular incidence [23,24], so that we expect an additional repulsion due to reflected energetic particles of less than 20% of the momentum received by the ions. Additionally, a similar effect would arise at high sheath voltages: sputtering of the surface becomes important and the sputtered particles would cause repulsion, too [25].

Now, we want to see if the above mentioned forces can explain the measured force. Figure 7a shows again the measured forces from Figure 5a, the electron pressure p_{e} and the sum $p_{\mathrm{e}} + p_{\mathrm{i}}$ of electron pressure as well as the pressure due to ions entering the sheath at Bohm velocity. Note, that p_{i} is actually an upper limit. The corresponding figure for the floating surface is Figure 7b. Again, the two cases do not differ qualitatively, so the following comments refer to both of them.

In case of $p = 20$ Pa, the predicted upper limit almost agrees with the measured forces, and one could conclude that the ions enter the sheath at Bohm velocity. However, the measured force at $p = 5$ Pa is about four to five times higher than the corresponding calculated upper limit.

This indicates that there must be yet another mechanism that causes momentum flux into the sheath. The only momentum transport by particles we still did not consider is the one due to the neutral gas atoms crossing the sheath boundary (see Fig. 6). In case of gas in thermal equilibrium, there would be no net momentum flux. However, the collisions of drifting ions in the presheath transferred momentum to a small fraction of neutral gas atoms. Estimates of this effect are difficult, since the scale length of the presheath and the electric field strength, especially in the complicated geometry of our experiment, are not known (see [26]).

Nevertheless, we can speculate that in the 5 Pa case the ion drift speed is $0.5v_{\mathrm{B}}$ which is in the range of sheath entry velocities predicted by various theories for the ratio $\lambda_{\mathrm{D}}/\lambda_{\mathrm{mfp}} \approx 0.25$ for the Debye length of $\lambda_{\mathrm{D}} = 200\,\mu$m (at $P_{\mathrm{rf}} = 300$ W) [21]. The kinetic energy of the drifting ions is then $\frac{1}{4}$ of the corresponding kinetic energy at Bohm speed, while the momentum is still $\frac{1}{2}v_{\mathrm{B}}m_{\mathrm{i}}$, i.e. half the corresponding momentum at Bohm speed. If the ion undergoes eight momentum exchange collisions, then the neutral collision partners would carry together eight times the ion momentum, or $4v_{\mathrm{B}}m_{\mathrm{i}}$. The knocked-on atoms start new collision cascades, similar to the case discussed for the sheath, whose branches would all end at the surface if the momentum is not carried away by thermal motion. A similar momentum enhancing effect was experimentally found in a radial plasma source which is similar to a Hall thruster in some aspects [11]. There, ion-neutral collisions caused an enhancement of the electric force exerted on the radial ion flow, too. For the radial plasma source, the electric field was known and the length of the ion acceleration region was clearly defined by the geometry of the device, which enabled calculations of the force. The enhancement of the imparted momentum was explained with the force effectively exerted on a larger mass consisting of ions and fast neutral atoms.

Now the question arises, why the force is not even higher in the 20 Pa case, since there are more collisions? There are two mechanisms which reduce the imparted momentum by collisions: the collisionality reduces the sheath entry velocity, which is much lower at 20 Pa than at 5 Pa (possibly down to $0.3v_{\mathrm{B}}$ [21]), and the repeated splitting of the momentum of the knocked-on atoms in the collision cascade, which happens about four times more often at the four times higher gas pressure (at similar widths of the presheaths), allows the momentum to be transported away from the surface by diffusion of the involved gas atoms.

5 Conclusions

An experiment was described where the force exerted by a low-pressure rf plasma on a test surface was measured. The test surface was one side of a cubic object immersed in the plasma, so that there was no plasma behind the test surface. The test surface was mounted on a pendulum whose deviations were measured with a camera. A calibration method has been described that uses the electrostatic attraction between the test surface and an additional second surface when a high voltage is applied to the pair of parallel plates.

The measured forces in the plasma have the order of magnitude of a few micronewtons and increase as the plasma density increases and decrease as the gas pressure increases. The electrically floating test surface experiences forces similar to the forces exerted on the grounded surface.

Several forces have been considered in order to understand the mechanism that causes the measured force. To this purpose, a simplified model was applied that consists of an electron-free plasma sheath and a quasi-neutral

presheath. The momentum flux was determined at the sheath edge, and three causes of momentum flux into the sheath where identified: first, the reflected electrons exerting the electron pressure, second, the ions entering the sheath with momentum, and third, the fast gas atoms entering the sheath with momentum gained in the presheath due to ion-neutral and subsequent neutral-neutral collisions. With the two first components, an upper limit for the force could be determined quantitatively based on data obtained by a Langmuir probe. These upper limits were smaller than the measured forces, so that it was concluded that the momentum influx from neutral gas atoms plays an important role. The trend that higher gas pressures yield lower forces was attributed to smaller sheath entering velocities of the ions and the diffusive loss of momentum that has been split many times by neutral-neutral collisions so that more knocked-on atoms became subthermal. The model explains the observation, that the two cases, the grounded and the electrically floating surface, do not experience much different forces: the relevant momentum flux appears at the sheath edge, and the wall potential determines only the position of the sheath edge, but not the momentum fluxes by ions, electrons and knocked-on atoms across the sheath edge.

Further investigations should aim at a simplified geometry, more supplementary diagnostics, and numerical plasma simulations. The setup described in this article is challenging for numerical simulations, because of the complex geometry which cannot be reduced to two or, better, one dimensions. This problem could be resolved by integration of the force probe and further diagnostics into a plane wall or an rf electrode. Suitable supplementary diagnostics are a retarding field analyzer and a calorimetric probe. The retarding field analyzer could determine the velocity distribution of the ions at the wall for a better knowledge of the ion pressure, and the calorimetric probe would be an alternative diagnostic which does not discriminate between ions and neutral atoms. Furthermore, a straightforward test of the here presented simple "sheath independent" model would be force measurements at bias voltages in a wider range, including high voltage.

References

1. J.A. Thornton, Thin Solid Films **54**, 23 (1978)
2. H. Kersten, D. Rohde, J. Berndt, H. Deutsch, R. Hippler, Thin Solid Films **377-378**, 585 (2000)
3. G. Makrinich, A. Fruchtman, J. Appl. Phys. **100**, 093302 (2006)
4. M. Stahl, T. Trottenberg, H. Kersten, Rev. Sci. Instrum. **81**, 023504 (2010)
5. S. Bornholdt, N. Itagaki, K. Kuwahara, H. Wulff, M. Shiratani, H. Kersten, Plasma Sci. Technol. **22**, 025019 (2013)
6. G.H. Wannier, Bell System Techical J. **32**, 170 (1953)
7. J. Heimerl, R. Johnsen, M.A. Biondi, J. Chem. Phys. **51**, 5041 (1969)
8. A. Palmero, J. Cotrino, C. Lao, A.R. González-Elipe, Phys. Rev. E **66**, 066401 (2002)
9. R.L. Stenzel, C. Ionita, R. Schrittwieser, J. Appl. Phys. **109**, 113305 (2011)
10. A. Greig, C. Charles, R. Hawkins, R. Boswell, Appl. Phys. Lett. **103**, 074101 (2013)
11. G. Makrinich, A. Fruchtman, Appl. Phys. Lett. **95**, 181504 (2009)
12. G. Makrinich, A. Fruchtman, Phys. Plasmas **21**, 023505 (2014)
13. K.-U. Riemann, J. Phys. D **24**, 493 (1991)
14. S.D. Baalrud, C.C. Hegna, J.D. Callen, Phys. Rev. Lett. **103**, 205002 (2009)
15. S.D. Baalrud, C.C. Hegna, Plasma Sources Sci. Technol. **20**, 025013 (2011)
16. S.D. Baalrud, C.C. Hegna, Plasma Sources Sci. Technol. **21**, 068002 (2012)
17. K.-U. Riemann, Plasma Sources Sci. Technol. **21**, 068001 (2012)
18. R.R.J. Gagn, A. Cantin, J. Appl. Phys. **43**, 2639 (1972)
19. V.A. Godyak, R.B. Piejak, B.M. Alexandrovich, J. Appl. Phys. **73**, 3657 (1993)
20. V.A. Godyak, V.I. Demidov, J. Phys. D **44**, 233001 (2011)
21. H.-B. Valentini, D. Kaiser, Plasma Sources Sci. Technol. **23**, 015004 (2014)
22. A.V. Phelps, J. Appl. Phys. **76**, 747 (1994)
23. N. Selden, N. Gimelshein, S. Gimelshein, A. Ketsdever, Phys. Fluids **21**, 073101 (2009)
24. E.D. Knechtel, W.C. Pitts, Astronautica Acta **18**, 171 (1973)
25. T. Trottenberg, A. Spethmann, V. Schneider, M. Stahl, M. Giesenhagen, Contrib. Plasma Phys. **52**, 584 (2012)
26. N.A. Almeida, M.S. Benilov, Phys. Plasmas **19**, 073514 (2012)